MODELING OF THE SYNTHESIS AND SUBSEQUENT GROWTH OF NANOPARTICLES IN DUSTY PLASMAS

Kathleen De Bleecker, and Annemie Bogaerts

PLASMANT, Dept. of Chemistry University of Antwerp,, Universiteitsplein 1, 2610 Wilrijk (Antwerp), Belgium

* Corresponding author: kathleen.debleecker@ua.ac.be, phone: +32 3 820 23 64, fax: +32 3 820 23 76

Abstract

The initial mechanisms of dust formation in radiofrequency acetylene (C_2H_2) plasmas are investigated by means of a self-consistent 1D fluid model Possible routes for particle growth are discussed and a comparison with particle formation in silane (SiH_4) discharges is made. The model considers a set of 39 species, including neutrals, radicals, ions and electrons, describing hydrocarbons (C_nH_m) containing up to 12 carbon atoms. Both successive anion/cation – molecule reactions seem to lead to a fast build up of the carbon skeleton

Keywords: particle formation, dusty plasmas, numerical modeling, nanoparticles

1. INTRODUCTION

Dust particles, from a few nanometers up to several micrometers, have been observed in many processing plasmas used for etching, sputtering or deposition of thin surface films. Until recently, the presence of dust was solely considered as a potential hazard, especially in the microelectronic and other surface processing technologies, as particles provide a significant source of film defects redeeming them as 'killer' particles. Therefore, early investigations mainly attempted at suppressing the particle growth or tried to avoid interference with the wafer surface. Currently, it seems that small particles can also have very interesting and useful properties, mainly due to their very small sizes (e.g. nanometer range), chemical composition or uniform size distribution [1,2]

In the photovoltaic cell production, for example, the creation and inclusion of nanocrystalline silicon particles in the intrinsic layer of amorphous hydrogenated silicon (a-Si:H), can result in a significant increase of the product quality [3]. The newly formed material shows improved transport properties and stability against the light induced effect, also known as the Staebler-Wronski effect. In order to obtain a controlled growth and deposition of these particles on the substrate material, we obviously must understand the mechanisms behind their origin and their behavior, including their transport, in the plasma. Comprehension of these aspects will help to advance the existent and future technological applications

In chemically active plasmas, such as silane (SiH_4) and acetylene (C_2H_2), it is generally believed that particle formation proceeds through a series of chemical reactions in the gas phase, better known as gas phase polymerization, whereby parent gas monomers are gradually transformed to macromolecules. Although the behavior of particles in the micrometer-sized regime is relatively well understood, the transition of gas species to particles remains a complex process, which is still open for investigation. These earlier stages, known as nucleation and coagulation, are of specific interest in current research. Besides investigations of the plasma chemistry, the dust particles will also acquire a negative charge due to the collection of plasma ions and electrons. The magnitude of the charge on a particle will greatly depend on the particle size and the plasma conditions. This negative charge will also be responsible for the confinement and consequently longer lifetimes of such particles in the plasma. Once the particles reach a certain size (i.e. several nanometers), other forces, besides the electric force and diffusion, will dominate their transport (e.g. the ion drag, the thermophoretic, and the neutral drag force). The competition between these different forces ultimately leads to the confinement of the particles in well-defined regions of the discharge [4,5]. In the end, particles will continue to grow until gravity drags them out of the discharge.

In this paper we will mainly discuss the chemical processes through which larger particles can be formed in a capacitively coupled acetylene (C_2H_2) RF discharge and try to identify the precursors of the dust formation with the use of a self-consistent one-dimensional (1D) fluid model. The gas phase discharge chemistry is investigated and the similarities and differences with particle formation in silane discharges are discussed.

2. MODEL DESCRIPTION

1. Fluid model

The model used in our calculations is based on the fluid model developed by Nienhuis et al. [6,7] for the description of a silane/hydrogen discharge. In the present paper, this model is used to investigate the nucleation of dust in an acetylene plasma. In the 1D fluid model the discharge is described by particle balance equations for the ions, electrons and neutrals, and an energy balance equation for the electrons. The electric field is calculated from the Poisson equation, which is coupled to the balance equations, making the model fully self-consistent. Power input into the plasma is transferred to the charged species (electrons and ions) by ohmic heating. Typical discharge quantities such as the electric field, densities and fluxes of the particles as a function of space and time are calculated self-consistently.

The most important aspects of the model will be given here. Further details concerning the numerical techniques and algorithms can be found elsewhere [8,9].

The density balance for each species j (electrons, ions, radicals and neutral molecules) is described by

$$\frac{dn_j}{dt} + \frac{d\Gamma_j}{dx} = S_j \tag{1}$$

where n_j and Γ_j are the particle's density and flux, respectively, and S_j represents the different source and sink terms of particle j (respectively formation/destruction). The gas inlet and pumping have been incorporated by the introduction of additional source and sink terms. The chemically inert molecules are perfectly mixed over the entire reactor volume. The radicals, on the other hand, can undergo reactions/transitions at the wall, resulting in a non-uniform profile.

The momentum balance is replaced by a drift-diffusion approximation, which means that each particle flux consists of two separate terms, a drift and a diffusion term

$$\Gamma_j = \mu_j n_j E - D_j \frac{dn_j}{dx} \tag{2}$$

where μ_j and D_j are the mobility and diffusion coefficient of species j, and E represents the electric field For the neutral particles the mobility term is equal to zero. Equation (2) assumes that the charged particles will react instantaneously to a change in the electric field. Because the ions can not follow the actual electric field, an effective electric field is taken into account which compensates the inertia effects originating from their lower momentum transfer frequency. An expression for the effective electric field is obtained by neglecting the diffusive transport and inserting the expression $\Gamma_i = \mu_i n_i E_{eff}$ in the simplified momentum balance

$$\frac{d\Gamma_i}{dt} = \frac{en_i}{m_i} E - \nu_{m,i}\Gamma_i, \tag{3}$$

where $\nu_{m,i}$ is the momentum transfer frequency of the ion i given by

$$\nu_{m,i} = \frac{e}{\mu_i m_i}. \tag{4}$$

Here e represents the elementary charge and m_i the mass of the ion. The effective electric field, replacing the instantaneous electric field in Eq. (2), is then given by

$$\frac{dE_{eff,i}}{dt} = \nu_{m,i}\left(E - E_{eff,i}\right) \tag{5}$$

The electric field E and the potential V are calculated using the Poisson equation

$$\frac{d^2V}{dx^2} = -\frac{e}{\varepsilon_0}\left(\sum n_+ - \sum n_- - n_e\right) \qquad E = -\frac{dV}{dx} \tag{6}$$

where ε_0 is the permittivity of free space, n_e the electron density, n_+ the total positive ion density and n_- the total negative ion density (the negative dust species included).

The electron energy density $w_e = n_e\varepsilon$ (i.e. the product of the electron density and the average electron energy) is calculated self-consistently from the second moment of the Boltzmann equation

$$\frac{dw_e}{dt} + \frac{d\Gamma_w}{dx} = -e\Gamma_e E + S_w \tag{7}$$

with Γ_w the electron energy density flux

$$\Gamma_w = \frac{5}{3}\mu_e w_e E - \frac{5}{3}D_e\frac{dw_e}{dx}, \tag{8}$$

and μ_e and D_e are the electron mobility and electron diffusion coefficients. The term S_w in Eq. (7) represents the loss of electron energy due to electron impact collisions. No energy balance is included for the ions and neutrals. The energy dissipated by the ions is only accounted for in the overall energy balance of the discharge, where a preset total consumed power is specified.

The system of non-linear differential equations is solved numerically. For the spatial discretization of the balance equations the Scharfetter-Gummel exponential scheme is used [10]. The computational grid is equidistant and contains 64 grid points. An implicit second order method [7] is applied to numerically treat the time evolution of the balance equations. Finally, the Newton-Raphson method is used to solve the resulting set of nonlinear equations. Convergence of the fluid model is reached when the relative changes of the discharge parameters between two succeeding RF cycles are less than 10^{-6}.

2. Plasma chemical kinetics

Particles in chemically active plasmas emerge as a result of numerous chemical processes in the ionized gas phase. In silane plasmas, anion-induced chain reactions are considered to be the main pathway leading to powder formation. Negative ions are generally believed to play a very important role in the dust formation, as they are confined by the sheath electric fields in the plasma bulk [11]. The long residence time of the anions in the plasma favors their further growth

and makes them good candidates to trigger particle formation. Previously we have developed a detailed chemical kinetics model for gas phase nucleation of hydrogenated silicon particles [12,13]. In that model dust is primarily formed by successive reactions of anions with silane molecules

$$Si_nH_{2n+1}^- + SiH_4^{(*)} \rightarrow Si_{n+1}H_{2n+3}^- + H_2 \quad (9a)$$

$$Si_nH_{2n}^- + SiH_4^{(*)} \rightarrow Si_{n+1}H_{2n+2}^- + H_2 . \quad (9b)$$

In addition to ground state SiH_4 molecules, reactions with vibrationally excited SiH_4 ($SiH_4^{(1-3)}$ and $SiH_4^{(2-4)}$) are also taken into account, as these species have sufficient internal energy to overcome probable energy barriers in some of the endothermic chain reactions [14]. The mechanism starts primarily from SiH_3^- and SiH_2^- anions, and includes silicon hydrides containing up to twelve silicon atoms. Other pathways involving e.g. positive ions can be excluded as a kinetic bottleneck is already formed at particles having relatively low numbers of silicon atoms, preventing the formation of positive ions having more than five or six silicon atoms [15].

Discharges in hydrocarbon mixtures also tend to produce dust, especially when a sufficient amount of acetylene is present [16]. In contrast to silane plasmas, the dust formation mechanisms in hydrocarbon discharges are much less understood and only a limited amount of data for hydrocarbon molecules is available. Therefore, various mechanisms have been proposed. Presumably both positive and negative ions play a role in the initial phase of the dust forming process, as mass spectrometry measurements reveal the same features in both the anion and cation mass spectra [17, 18].

In this paper acetylene is considered as an example of the hydrocarbon discharge chemistry, as it yields more highly polymerized ions than methane (CH_4) and also has a much stronger and faster tendency to form dust. Table 1 gives an overview of the 39 different species considered in the acetylene model, besides the electrons. Starting from C_2H_2 a series of chemical reactions has been gradually incorporated in the 1D fluid model that leads to the formation of larger hydrocarbons (C_nH_m) containing up to a maximum of 12 carbon atoms. The absence of

hydrocarbon molecules with an odd number of carbon atoms is a distinct feature of acetylene discharges. The typical spectral pattern in mass spectrometric measurements shows clear sequences of ions with even numbers of carbon atoms indicating that the strong carbon bond structure ($H-C\equiv C-H$) of the initial acetylene molecule persists upon successive insertion of acetylene in the hydrocarbon species.

Table 1. *Different species taken into account in the hydrocarbon model, besides the electrons*

Molecules	Ions	Radicals
C_2H_2	$C_2H_2^+$, C_2H^+, CH^+, C_2^+, C^+	CH, CH_2
C_4H_2, C_6H_2, C_8H_2	$C_4H_2^+$, $C_6H_2^+$, $C_6H_4^+$, $C_8H_6^+$	
$C_{10}H_2$, $C_{12}H_2$	$C_{10}H_6^+$, $C_{12}H_6^+$	
		C_2H_3, C_4H_3, C_6H_3
	C_2H^-, C_4H^-, C_6H^-, C_8H^-	C_2H, C_4H, C_6H, C_8H
	$C_{10}H^-$, $C_{12}H^-$	$C_{10}H$, $C_{12}H$
H_2	H_2^+, H^+	H

While in our model for silane plasmas the positive ions could be limited to three different species, i.e. SiH_3^+, $Si_2H_4^+$ and H_2^+ [13], both the positive and negative ions in the acetylene model are extended up to hydrocarbons containing 12 carbon atoms, as the role of both pathways in the first step of particle formation can not be excluded. In the model we account for a total of 78 volume reactions comprising 22 electron impact reactions with acetylene and hydrogen, 35 ion-neutral reactions (anion or cation – acetylene reactions and mutual anion-cation neutralization reactions) and 21 neutral-neutral reactions (hydrogen abstraction, C_2H insertion). Since detailed data on many processes in an acetylene discharge is still lacking, some assumptions have to be made which are tested against the data known from the experimentally obtained mass spectra. Below a comprehensive summary is given of the most important part of the reaction mechanism.

2.2.1 Reactions involving anions

Usually negative ions are not considered in the modeling of 'standard' acetylene discharges, i.e. without the inclusion of dust formation [14,15]. However, the primary C_2H^- ion, formed through the dissociative attachment of C_2H_2, can be incorporated in neutral species, thereby creating larger negative ions which can eventually grow to nanometer and micrometer sized particles that remain trapped in the plasma due to their large negative charge. In spite of the difficulty of adding an electron to the filled valence shell of acetylene, the electron affinity of the C_2H radical seems to be sufficiently large to produce a stable C_2H^- anion

$$e^- + C_2H_2 \rightarrow C_2H^- + H \tag{10}$$

This dominant anion is the first species of the particle formation and can in turn undergo the following anion-molecule chain reactions:

$$C_2H^- + C_2H_2 \rightarrow C_4H^- + H_2 \tag{11a}$$

$$C_4H^- + C_2H_2 \rightarrow C_6H^- + H_2 \tag{11b}$$

...

$$C_{2n}H^- + C_2H_2 \rightarrow C_{2n+2}H^- + H_2 \tag{11c}$$

High resolution mass spectra [12] show that the majority of the anions in C_2H_2 plasmas are nearly pure carbon anions, hence, in accordance with the analogous path in silane discharges, molecular hydrogen is lost in every polymerization reaction. Only anions with an even carbon atom number are included in the model, as the triple carbon bond of acetylene is preserved.

No precise rate coefficients for anion chain reactions can be found in literature, but a theoretical upper limit for ion-molecule reactions can be predicted by the Langevin collision rate constant k_L [16]:

$$k_L = e\left(\frac{\pi}{\varepsilon_0}\right)^{1/2}\left(\frac{\alpha}{m_r}\right)^{1/2} \tag{12}$$

where α is the neutral atom or molecule polarizability (in $Å^3$) and m_r is the reduced mass (in amu) of the two reacting species Inserting the polarizability of 3 49 $Å^3$ for acetylene [17] results in a Langevin rate of the order of 10^{-15} m^3 s^{-1} However, since these rate constants represent an upper bound for the actual reaction rates, we have used, according to experimental data in [18], Langevin rate constants reduced by three orders of magnitude in our modeling study, i.e values of the order of 10^{-18} m^3 s^{-1}. Taking larger reaction rates would result in an increase in concentration with rising carbon atom number, which is not in agreement with the observed high resolution mass spectra [12].

2.2.2 Cation-molecule reactions

In contrast to silane plasmas, the hydrocarbon positive ions polymerize to the same extent as the negative ions and, hence, can not be excluded as a possible route of powder formation. Positive ions are formed from acetylene by electron impact ionization, creating mostly $C_2H_2^+$ Starting from $C_2H_2^+$ rapid condensation reactions with acetylene yield the production of higher mass hydrocarbon cations with or without subsequent loss of molecular or atomic hydrogen The principal reaction sequence can be summarized by:

$$C_2H_2^+ \xrightarrow{C_2H_2} \underset{(+H_2)}{C_4H_2^+} \xrightarrow{C_2H_2} C_6H_4^+ \xrightarrow{C_2H_2} C_8H_6^+ \xrightarrow{C_2H_2} \underset{(+H_2)}{C_{10}H_6^+} \xrightarrow{C_2H_2} etc. \tag{13}$$

The specific ionic product obtained from any given ion-acetylene reaction, and thus the degree of hydrogenation, depends upon the extent of stabilization achieved by the chemical intermediate [19, 20]. The primary reaction between $C_2H_2^+$ and C_2H_2 can for example lead to $C_4H_2^+$ and $C_4H_3^+$ production $C_4H_3^+$ is not considered as a separate species in the model; however its production is intrinsically incorporated in $C_4H_2^+$ by using the overall reaction rate constant of both reaction channels, i.e. 1.2×10^{-15} m^3 s^{-1} [21]. Another fragment ion generated from acetylene ionization, i.e. C_2H^+, also reacts with C_2H_2 to give $C_4H_2^+$

$$C_2H^+ + C_2H_2 \rightarrow C_4H_2^+ + H \quad (14)$$

with the fast rate constant of 1.7×10^{-15} m^3 s^{-1} [20]. C^+, C_2^+ and CH^+ ions are also formed through dissociative ionization of acetylene, and can in principle react with C_2H_2 via condensation with loss of H or H_2. Although all these reactions are rapid with rate constants close to the collision limit, these reactions are not taken into account in the model, since the initial formation of these species is too low to make these reactions efficient.

Besides fast polymerization reactions, mutual ion-ion neutralization represents another loss process for both the anion and cation molecules. The rate constant for neutralization is taken from [22] and is only weakly dependent on the nature of the molecule, resulting in our case in a reaction rate constant of 8.7×10^{-14} m^3 s^{-1}.

2.2.3 Neutral chemistry

Breakage of a C-H bond in acetylene by electron impact dissociation produces the C_2H radical that can in turn be inserted into hydrocarbons to produce larger $C_{2n}H_2$ molecules

$$C_2H + C_{2n}H_2 \rightarrow C_{2n+2}H_2 + H \quad (15)$$

The reaction chain is initiated by the insertion of C_2H into acetylene leading to the formation of diacetylene (C_4H_2) and atomic hydrogen. A corresponding $C_{2n}H$ radical can be formed by electron induced dissociation of the $C_{2n}H_2$ molecule and can play a role in the deposited layer. The deposition process itself is described by a sticking model that ensures that the loss of species due to plasma-wall interactions is taken into account.

III. RESULTS AND DISCUSSION

A typical parallel-plate PECVD reactor has been modeled with an inter-electrode spacing of 3 cm at a discharge frequency of 13.56 MHz. The capacitively coupled RF plasma is operated at a total

gas pressure of 40 Pa, a power of 5 W and a gas temperature of 400 K, with a gas flow of 20 sccm of pure acetylene or silane. Figure 1 presents the calculated densities of the electrons and the most abundant positive and negative ions in a pure acetylene (a) and a pure silane discharge (b) as a function of position in the plasma. Near the sheaths a slight time variation of the ion profiles can occur, hence, time-averaged electron and ion densities have been plotted.

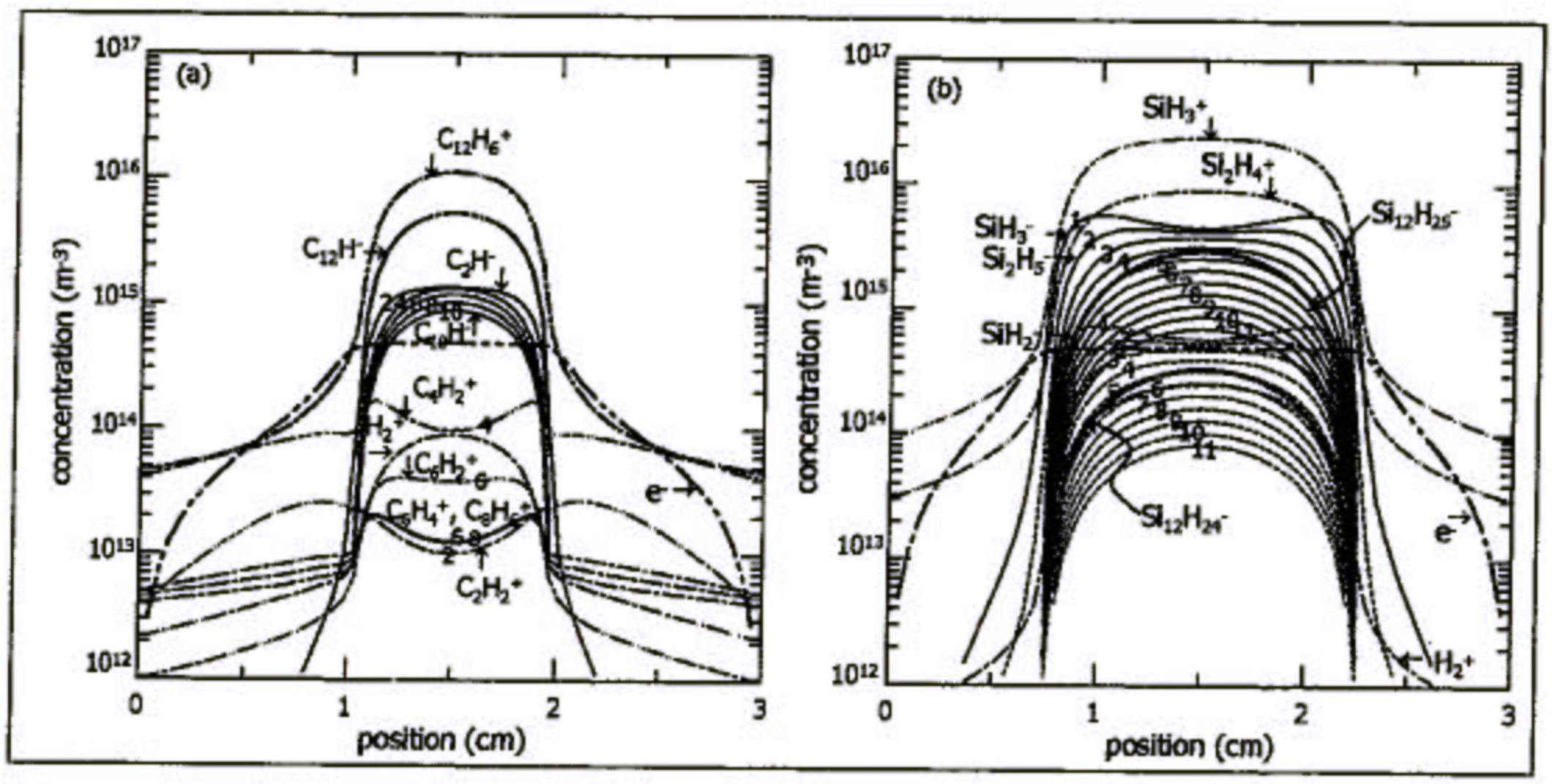

Figure 1. *Density profiles of ions in an acetylene (C_2H_2) discharge (a); and a silane (SiH_4) discharge (b); at a pressure of 40 Pa, a power of 5 W and 13.56 MHz.*

In the acetylene plasma (Fig. 1a) two different pathways involving positive or negative ions, respectively, can be distinguished. The number indicated on every anion plot specifies the number of carbon atoms. In each pathway a gradually decreasing trend can be observed with increasing number of carbon atoms. This is in good agreement with the observed mass spectra in [12] where the same trend can be detected. In the model both chains are stopped at hydrocarbon ions containing 12 carbon atoms. Therefore, $C_{12}H_6^+$ and $C_{12}H^-$ appear to be the most prominent species formed in the plasma which represent the final accumulating stage and thus symbolize the

sum of all larger cations or anions, respectively. Since most cation-acetylene reactions proceed at a rate close to the collision limit (see above) lower concentrations of the intermediate hydrocarbon positive ions are produced in comparison to the intermediates in the anion chain, where the reactions proceed at a rate constant close to 10^{-18} m^3 s^{-1}. The cation density profiles exhibit a lower density in the plasma bulk which is probably a direct consequence of the fast loss processes, i.e. association reactions with C_2H_2, which can not be entirely compensated by the slow movement of the positive ions towards the plasma center. In the figure only the most dominant positive hydrocarbons are shown. Other positive ions formed through the dissociative ionization of acetylene, i.e. C^+, C_2^+ and CH^+, reach a concentration of approximately 10^{10} m^{-3} (not shown). $C_4H_2^+$ appears to be the most abundant positive ion followed by $C_6H_2^+$ and $C_6H_4^+$. This is also seen in mass spectra which peak at ions containing 4 and 6 carbon atoms.

For comparison the electron and ion profiles in a silane plasma are shown in Fig. 1(b). The major positive ion appears to be SiH_3^+ with a density of about 2×10^{16} m^{-3} in the center of the discharge. In experimental data no cation powder route can be observed, hence, only two other positive ions are considered in the model, i.e. $Si_2H_4^+$ and H_2^+. For the anions, however, two different routes can be discerned, starting from either SiH_3^- or SiH_2^- [see Eqs. 1(a) and 1(b) above]. Similar to the acetylene plasma, the anions are mostly confined to the bulk of the discharge since they are repelled by the high electric fields in the plasma sheaths, and they show a general decreasing trend towards larger numbers of silicon atoms (apart from the final $Si_{12}H_{25}^-$ and $Si_{12}H_{24}^-$ stages which represent the sum of all larger anions). The rate coefficient for the anion reactions (~10^{-18} m^3 s^{-1}) is similar to the one used in the acetylene anion chemistry. It is clear from Fig. 1(b) that mainly the SiH_3^- pathway, represented by solid lines, will create higher mass silicon hydrides and less than 10% of the particle formation proceeds through the SiH_2^- pathway, depicted by dashed lines.

In Figure 2 the calculated concentrations of the various hydrocarbon molecules (a) and radicals (b) in the acetylene discharge are shown at the same conditions as discussed above. The densities of the background neutrals are homogeneously distributed over the entire reactor and are produced in larger amounts compared to their corresponding radicals. Similar to the ion density profiles higher mass hydrocarbon molecules show a decreasing trend with increasing number of carbon atoms.

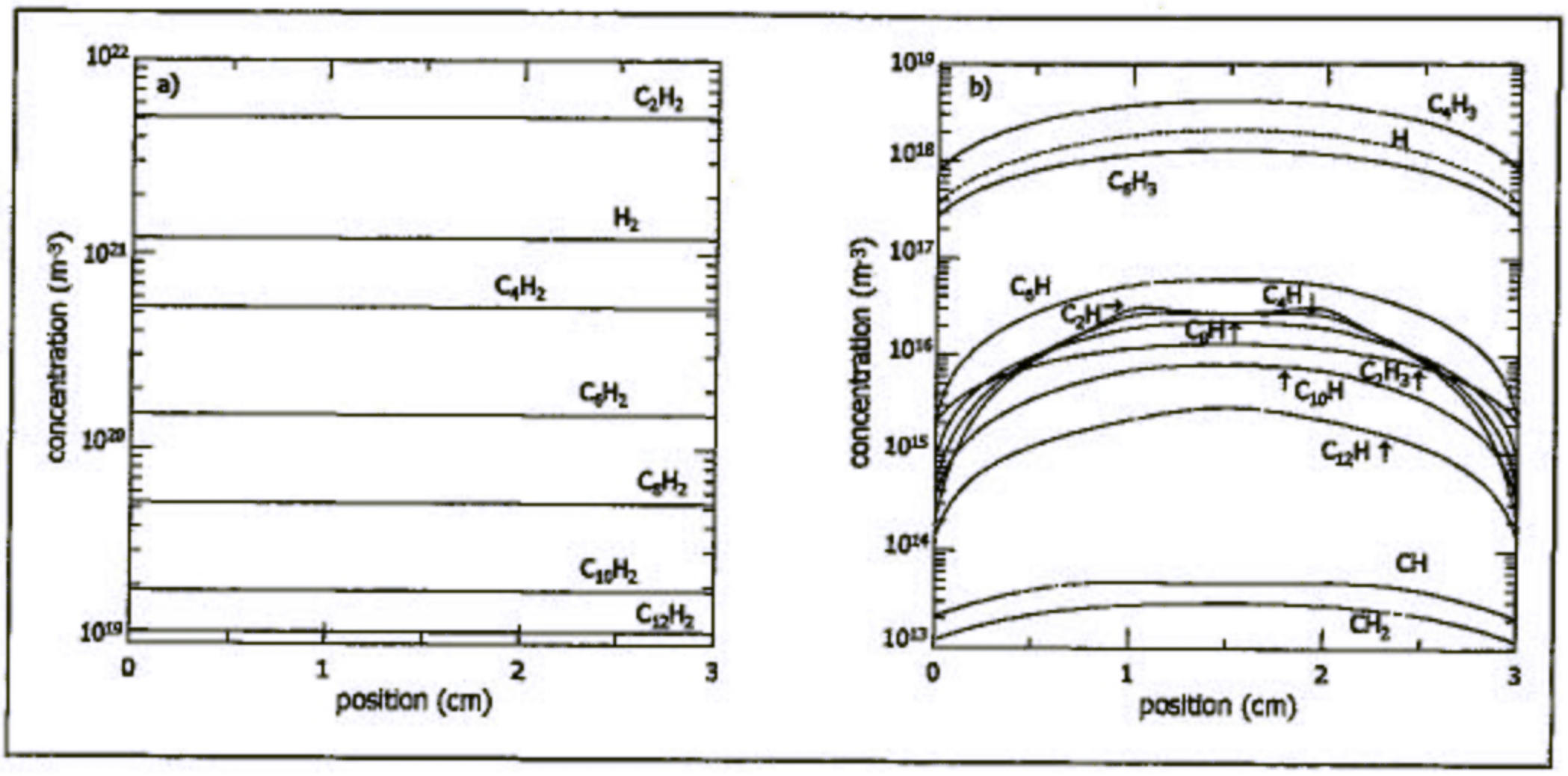

Figure 2. *Density profiles of the various hydrocarbon molecules (a); and radicals (b) in an acetylene discharge; at a pressure of 40 Pa, 5 W and 13.56 MHz.*

The acetylene background gas is present at the highest density and takes a value of 4×10^{21} m^{-3} Other non-ionic gaseous products that can be found at high concentrations in the acetylene discharge are diacetylene (C_4H_2) and molecular hydrogen. The high H_2 concentration comes from the many chemical reactions that produce molecular hydrogen as a side product (see above).

All twelve radicals are depicted in Figure 2(b) and mostly encompass carbon rich species C_nH_m (with $n > m$). The radicals are typically characterized by their decreasing density towards the electrodes, representing their reactivity at the walls. A large amount of atomic hydrogen is present with a density of ~ 1×10^{18} m^{-3}.

IV. CONCLUSIONS

The synthesis and subsequent growth of nanoparticles in a low pressure capacitively coupled acetylene (C_2H_2) discharge has been investigated with a self-consistent one-dimensional fluid

model. With the developed fluid model we have tried to identify the precursors of the dust formation by investigating the carbonaceous gas phase discharge chemistry and comparing its similarities and differences with particle formation in silane discharges. From our results we can conclude that more pathways towards dust formation exist for acetylene plasmas. Indeed, both positive ions, starting from $C_2H_2^+$, and negative ions, starting from C_2H^-, derived from acetylene may participate as precursors to dust formation, while in silane processing discharges the anions, and more specifically SiH_3^-, are the likely precursors of powder formation. Once the particles reach the nanometer size the negative ions will however probably again persist as the most important dust precursors, since they remain trapped in the discharge due to their large negative charge, while the positive ions will likely be extracted from the discharge before they can grow any further.

V. ACKNOWLEDGMENTS

K. De Bleecker is indebted to the Institute for the Promotion of Innovation through Science and Technology in Flanders (IWT-Vlaanderen) for financial support.

References

1. A. Bouchoule, in Dusty Plasmas: Physics, Chemistry and Technological Impacts in Plasma Processing, edited by A. Bouchoule (Wiley, Chichester, UK, 1999).
2. S. V. Vladimirov, and K. Ostrikov, "Dynamic self-organization phenomena in complex ionized gas systems: new paradigms and technological aspects," Phys. Reports **393**, 175 (2004).
3. Y. Poissant, P. Chatterjee, and P. Roca i Cabarrocas, "Analysis and optimization of the performance of polymorphous silicon solar cells: experimental characterization and computer modeling," J. Appl. Phys. **94**, 7305 (2003).
4. K. De Bleecker, A. Bogaerts, and W. Goedheer, "Modeling of the formation and transport of nanoparticles in silane plasmas," Phys. Rev. E **70**, 056407 (2004).

5. K. De Bleecker, A. Bogaerts, and W. Goedheer, "Role of the thermophoretic force on the transport of nanoparticles in dusty silane plasmas," Phys Rev **71**, 066405 (2005).

6. G. J. Nienhuis, W. J. Goedheer, E. A. G. Hamers, W. G. J. H. M. van Sark, and J. Bezemer, "A self-consistent fluid model for radio-frequency discharges in SiH_4-H_2 compared to experiments," J. Appl. Phys. **82**, 2060 (1997).

7. G. J. Nienhuis, "Plasma models for silicon deposition," Ph.D. thesis, Utrecht University, 1998.

8. J. D. P. Passchier, "Numerical fluid models for RF discharges," Ph.D. thesis, Utrecht University, 1994.

9. J. D. P. Passchier, and W. J. Goedheer, "Relaxation phenomena after laser-induced photodetachment in electronegative rf discharges," J. Appl. Phys. **73**, 1073 (1993).

10. D. L. Sharfetter, and H. K. Gummel, "Large-signal analysis of a silicon read diode oscillator," IEEE Trans. Electron Devices **16**, ED-64 (1967).

11. A. A. Howling, L. Sansonnens, J-L. Dorier, and Ch. Hollenstein, "Negative hydrogenated silicon ion clusters as particle precursors in RF silane plasma deposition experiments", J. Phys. D: Appl. Phys. **26**, 1003 (1993).

12. K. De Bleecker, A. Bogaerts, W. Goedheer, and R. Gijbels, "Investigation of growth mechanisms of clusters in a silane discharge with the use of a fluid model," IEEE Trans. Plasma Sci. **32**, 691 (2004).

13. K. De Bleecker, A. Bogaerts, R. Gijbels, and W. Goedheer, "Numerical investigation of particle formation mechanisms in silane discharges," Phys. Rev. E **69**, 056409 (2004).

14. A. A. Fridman, L. Boufendi, T. Hbid, B. V. Potapkin, and A. Bouchoule, "Dusty plasma formation: Physics and critical phenomena. Theoretical approach," J. Appl. **79**, 1303 (1996).

15. M. L. Mandich, W. D. Reents, Jr., and K. D. Kolenbrander, "Sequential clustering reactions of SiD_3^+ with SiD_4 and SiH_3^+ with SiH_4: another case of arrested growth of hydrogenated silicon particles," J. Chem. Phys. **92**, 437 (1990).

16. S. Hong, J. Berndt, and J. Winter, "Growth precursors and dynamics of dust particle formation in the Ar/CH_4 and Ar/C_2H_2 plasmas," J. Phys. D: Appl. Phys. **12**, 46 (2003).

17 Ch Deschenaux, A Affolter, D Magni, Ch Hollenstein, and P Fayet, " Investigations of CH4, C2H2 and C2H4 dusty RF plasmas by means of FTIR absorption spectroscopy and mass spectrometry," J Phys D: Appl Phys **32**, 1876 (1999)

18 Ch Hollenstein, W Schwarzenbach, A A Howling, C Courteille, J-L Dorier, and L Sansonnens, "Anionic clusters in dusty hydrocarbon and silane plasmas, " J Vac Sci Technol A **14**, 535 (1996)

19 J R Doyle, "Chemical kinetics in low pressure acetylene radio frequency glow discharges," J Appl Phys **82**, 4763 (1997)

20 D Herrebout, A Bogaerts, R Gijbels, W J Goedheer, and A Vanhulsel, "A one-dimensional fluid model for an acetylene RF discharge: a study of the plasma chemistry," IEEE Trans Plasma Sci **31**, 659 (2003)

21 J Perrin, O Leroy, and M C Bordage, "Cross-sections, rate constants and transport coefficients in silane plasma chemistry," Contrib Plasma Physics **36**, 3 (1996)

22 C J F Böttcher, and P Borderwijk, *Theory of electric polarization*, Elsevier, Amsterdam (1978)

23 J Perrin, C Böhm, R Etemadi, and A Lloret, "Possible routes for cluster growth and particle formation in RF silane discharges," Plasma Sources Sci Technol **3**, 252 (1994)

24 M J Vasile, and G Smolinsky, "The chemistry of radiofrequency discharges: acetylene and mixtures of acetylene with helium, argon and xenon," Int J Mass Spectrom Ion Phys **24**, 11 (1977)

25 V G Anicich, W T Huntress, Jr., and M J McEwan, "Ion-molecule reactions of hydrocarbon ions in C_2H_2 and HCN," J Phys Chem **90**, 2446 (1986)

26 J S Knight, C G Freeman, M J McEwan, V G Anicich, and W T Huntress, Jr., "A flow tube study of ion-molecule reactions of acetylene," J Phys Chem **91**, 3898 (1987)

27 S Stoykov, C Eggs, and U Kortshagen, "Plasma chemistry and growth of nanosized particles in a C2H2 RF discharge," J Phys D: Appl Phys **34**, 2160 (2001)